29th EPS Conference on Plasma Phys. and Contr. Fusion Montreux, 17-21 June 2002 ECA Vol. ***26B****, P-5.095 (2002)*

Interpretation of ECE measurements on MAST

J. Preinhaelter[1)], V. Shevchenko[2)], M. Valovic[2)], P. Pavlo[1)], L. Vahala[3)], G. Vahala[4)], and the MAST team[2)]

1) *EURATOM/IPP.CR Association, Institute of Plasma Physics, 182 21 Prague, Czech Republic*
2) *EURATOM/UKAEA Fusion Association, Culham Science Centre, Abingdon, OX14 3DB, UK*
3) *Old Dominion University, Norfolk, VA 23529, USA*
4) *College of William & Mary, Williamsburg, VA 23185, USA*

Introduction. Extensive ECE data from 16 to 75 GHz are available in MAST. The characteristic low magnetic field and high plasma density of a spherical tokamak do not permit the typical radiation of O and X modes from the first five electron cyclotron harmonics. Thus only electron Bernstein modes, (modes not subject to a density limit) which mode convert into the electromagnetic waves in the upper hybrid resonance region, can be responsible for the measured radiation.

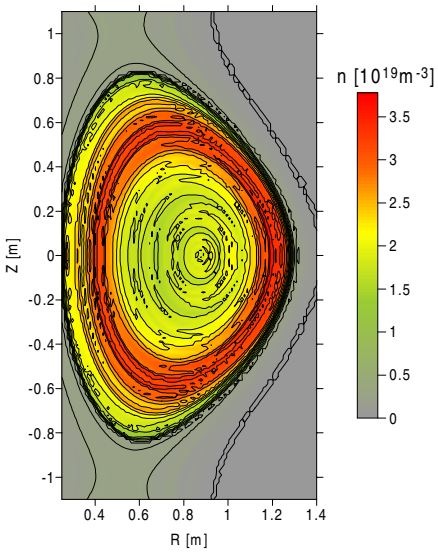

Fig. 1 Plasma density in RZ cross-section in MAST for shot #4958 at t=120ms

Wave propagation model. To interpret the experimental results we develop a realistic 3D model of the MAST plasma. The instantaneous magnetic field and its spatial derivatives are reconstructed from a 2D splining of two potentials determined by an EFIT equilibrium reconstruction code, assuming toroidal symmetry. The plasma density (Fig. 1) and temperature profiles in the whole RZ cross-section of the plasma are obtained from mapping the high spatial resolution Thomson scattering measurements on the magnetic surfaces and then interpolating between the low and high field sides values.

The intersection of the antenna pattern with the separatrix determines both the spot position (at which the antenna is aimed) as well as the components of wave vector of the outgoing waves (see Fig. 2). Only linearly polarized waves are detected and the plane of polarization can be selected by the orientation of the polarization rotator [5]. Since we wish to detect the emission of oblique O-modes the ECE antenna is oriented so that the at the plasma boundary the wave vector and the electric field vector of outgoing waves are lying in the plane spanned by the edge density gradient and the magnetic field vectors.. In Fig. 2 we also show the auxiliary plane-stratified slab of plasma which will be used in the subsequent numerical full wave solution of wave propagation.

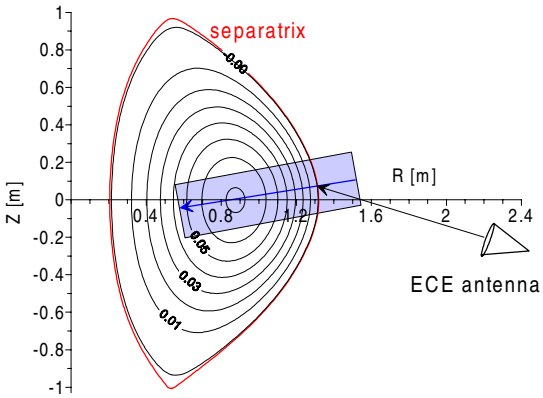

Fig. 2. Antenna position. The direction of view is inclined about 16° from the equatorial plane upward and the angle between its projection to the equatorial plane and the vertical plane going through the tokamak axis and the antenna position is about 20°.

A global schematic picture of wave propagation in the MAST plasma is shown in Fig. 3. The O- and X-mode cut-offs and resonances are derived from a WKB approximation for the propagation

of O and X modes in an auxiliary plane-stratified cold plasma slab. We see that the O-and X-modes can propagate only near the plasma boundary and they penetrate only slightly into the transport barrier, which was formed in this shot during its H-mode phase.

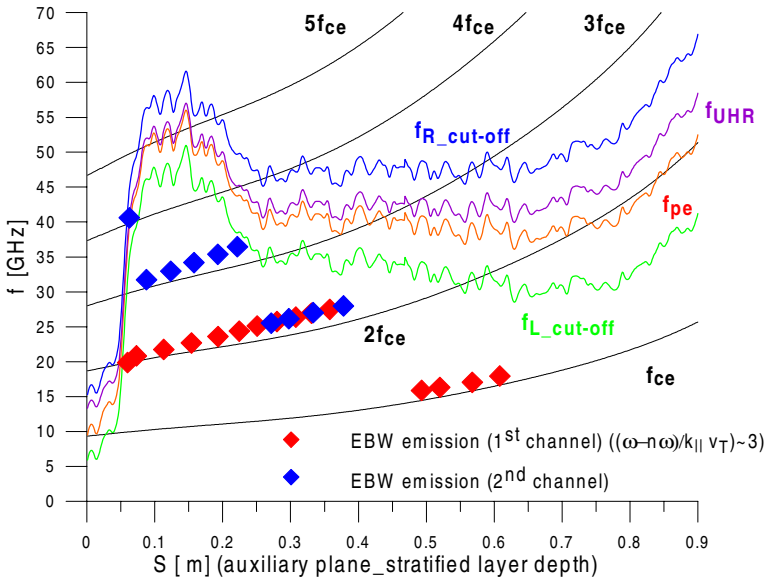

Fig. 3. Cut-offs and resonances in MAST. Depth S is measured along the normal to the separatrix at the spot of the antenna pattern. Separatrix is at S=0.02m because of the 0.02m SOL.

Since this region is only several centimeters thick the plane- stratified cold plasma model can be used for the description of the full wave solution of the X-O mode conversion at the plasma resonance region [1], [2]. We find that the power in the linearly polarized plasma emission received by the antenna beam decreases with the frequency increase (see Fig.4). We have assumed that the X-mode, of unit power, is incident at the upper hybrid resonance (UHR) region. At low frequencies, the efficiency for X-O conversion is practically 100% at the plasma resonance region. Since the mode-converted oblique O mode is almost circularly polarized, the intensity of the detected linearly polarized fraction will be practically one half of this value. At high frequencies the mode conversion efficiency is reduced because the width of the evanescent region becomes comparable to the wavelength.

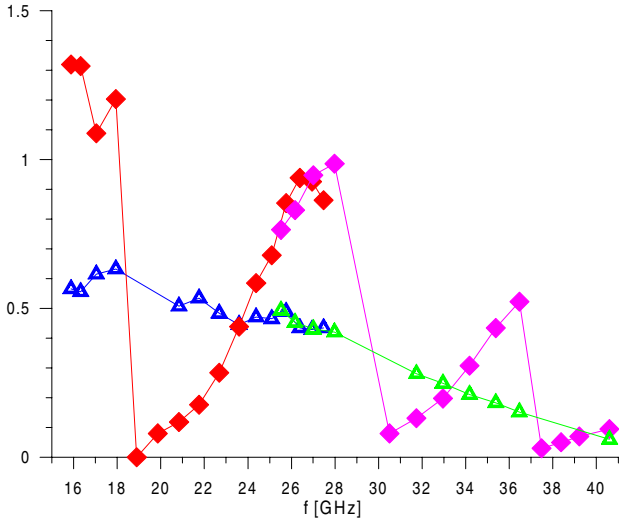

Fig. 4. Intensity of linearly polarized fraction of the O-mode emitted at oblique incidence of unit power EBW ($C_{EBW-X-O}$) from plasma interior (triangles). Temperature (diamonds, [keV]) of the black body EBW source.

In the central part of the plasma only the EBW can propagate. Because EBW is fully converted to the X-mode in the UHR region, only the intensity of the EBW emission from the electron cyclotron regions remains to be determined. If the plasma in these central regions is in thermodynamic equilibrium we can use the Rayleigh-Jeans law for the intensity of black body radiation: $I_{EBW} \sim T_e \omega^2$. Thus, we must determine for each frequency the position at which the EBW is absorbed. Since ray–tracing of EBW gives the most reliable results we have begun to modify our lower hybrid wave code [3] to handle EBW. These results will be presented elsewhere. In this paper, we investigate the propagation of EBW in our auxiliary plane stratified plasma slab (see Fig. 2). Because the EBW's are almost electrostatic we solve the following dispersion relation [4]:

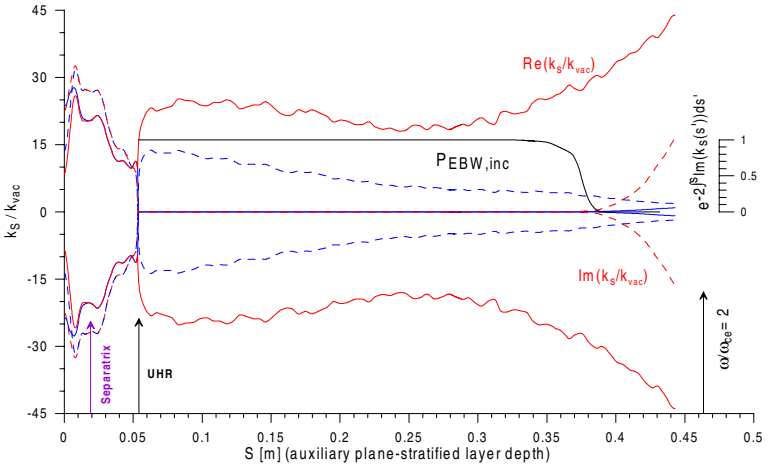

Fig. 5. Profile of EBW wave vector component k_S parallel to density gradient ($k_\perp=\sqrt{(k_S^2+k_{pol}^2)}$, f=27.98GHz, at the plasma boundary k_{par}/k_{vac}=-0.66, k_{pol}/k_{vac}=-0.038, #4958, t=120ms). Blue dashed lines correspond to the non-physical long wavelength branch of electrostatic waves. The black line is incident (from UHR) unit EBW power. The wave is fully absorbed at S= 0.38m where T=0.99keV

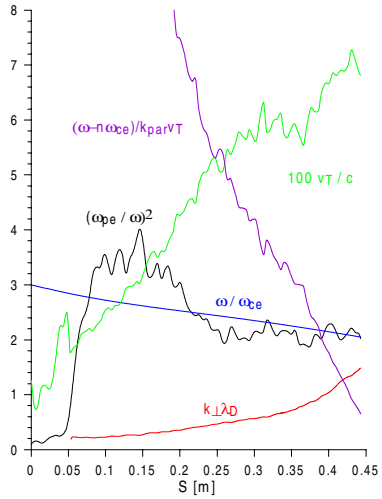

Fig. 6. Profiles of plasma parameters along the depth S. Absorption (or emission) of EBW is reached for $(\omega - n\ \omega_{ce})/ k_{par}\sim 3$.

$$D \equiv 1+\frac{2\omega_0^2}{k^2 v_T^2}\left(1+\sum_{n=-\infty}^{\infty}\frac{\omega}{|k_{par}|v_T}Z\left(\frac{\omega-n\omega_{ce}}{|k_{par}|v_T}\right)e^{-z_L}I_n(z_L)\right)=0,$$

where Z is the plasma dispersion function, $z_L=(k_{perp}v_T/\omega_{ce})^2/2$, $v_T=2T_e/m_e$ the electron thermal velocity, I_n the modified Bessel function, ω the wave frequency, $\omega_0(R,Z)$ the local plasma frequency, $\omega_{ce}(R,Z)$ the local electron cyclotron frequency, and k_{par} and k_{perp} are components of the wave vector parallel and perpendicular to the local magnetic field. In Fig. 5 we plot the

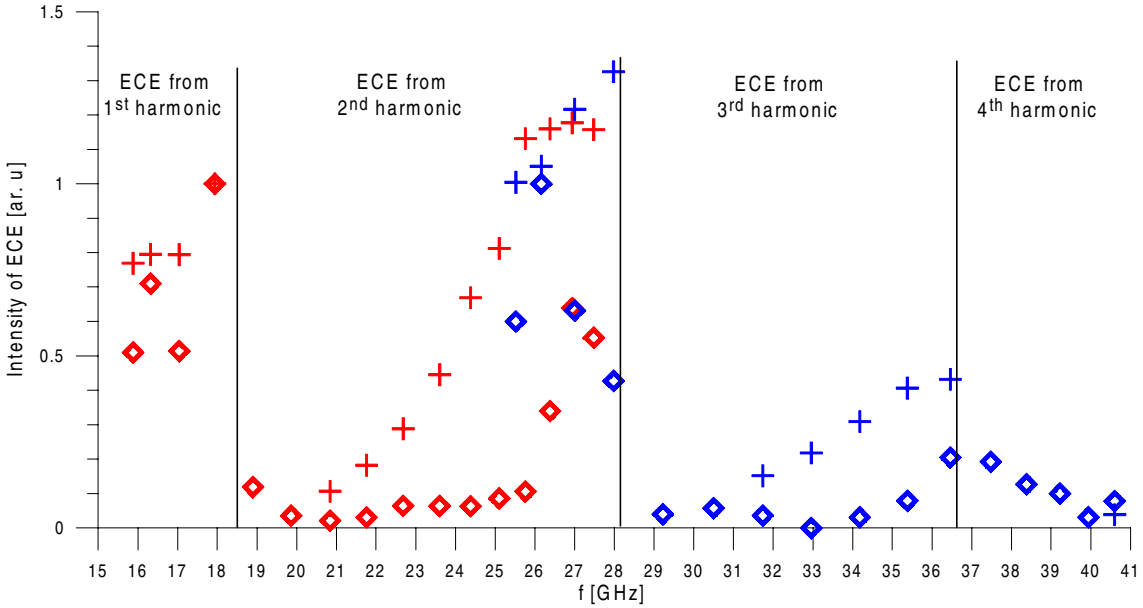

Fig 7. ECE from MAST for # 4958 at t=120ms. **Diamonds** are experimental data for 34 frequencies in two bands (16-27 red and 27-40 blue) and **crosses** are our estimates of ECE intensity for the same frequencies. As a reference frequency f=17.94 was chosen.

solution of D=0 for complex k_{perp}. Maximum emission is obtained for frequencies that are slightly below the electron cyclotron frequency at the plasma surface. In this case the EBW is emitted deep in the plasma central region where the temperature is high (see Fig 4).

Interpretation of emission spectra. Because of relatively low plasma density in the shot 4958, the plasma emission was reliably observed in the first two frequency bands (16-26GHz and 26-40GHz) of the frequency scanning EBW radiometer [5]. In Fig. 7 we compare the measured ECE intensity at t=120ms when the density and the temperature were measured by Thomson scattering. We normalized the estimated intensities of ECE with respect to the same frequency f_{ref}=17.94GHz ($T_{EBWemission}$=1.2keV, $C_{EBW\text{-}X\text{-}O}$=0.632) as the experimental data:

$$I_{ECE}(f) = \frac{C_{EBW-X-O}(f)}{C_{EBW-X-O}(f_{ref})} \frac{T_{EBWemission}(f)}{T_{EBWemission}(f_{ref})} \frac{f^2}{f_{ref}^2}$$

We see that the frequency dependence of ECE splits into regions which corresponds to radiation from subsequent electron cyclotron harmonics. The agreement between the experimental data and our estimates is only qualitative, with the measured emission substantially weaker for frequencies lying in the first two thirds of the interval (Fig. 7) between the electron cyclotron harmonics. This can be partially attributed to the penetration of EBW into a rarefied plasma (for frequencies slightly above EC harmonics at the plasma edge) where the plasma is cold and collisional damping may be important (see Fig. 8). Moreover the factor $k_\perp \lambda_D$, for these frequencies, is comparable with unity even in the UHR region so that the existence of EBW is questionable. Note that an increase in k_{par}, predicted in a ray tracing calculation of EBW propagation in a 3D plasma [6], can shift the absorption-emission region substantially to lower T. Also the non-monotonic magnetic field profile caused by the bootstrap current in the transport barrier region can shift the resonance on EC harmonics nearer to the plasma surface.

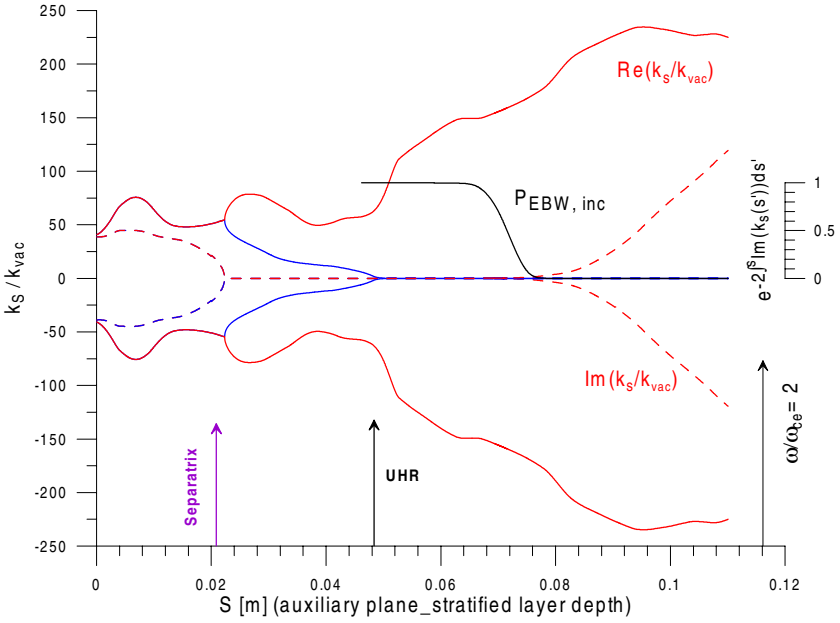

Fig. 8. Profile of EBW wave vector component k_S parallel to density gradient ($k_\perp=\sqrt{(k_S^2+k_{pol}^2)}$, f=20.84GHz,at the plasma boundary k_{par}/k_{vac}=-0.66, k_{pol}/k_{vac}=-0.038, #4958, t=120ms)

The work was partly supported by the Grant No. 202/00/1215 of Czech Grant Agency.
The UK Dept. of Trade and Industry and Euratom jointly fund the MAST program.

References

[1] J. Preinhaelter, V. Kopecky, J. Plasma Phys. 10, 1 (1973), part 1
[2] M.A. Irzak et al., Plasma Physics Reports 25, 601 (1999).
[3] T. H. Stix, Waves in Plasmas, AIP, New York, 1992.
[4] P. Pavlo, L. Krlin, Z. Tluchor, Nucl. Fusion, Vol. 31, (1991), 711
[5] V. Shevchenko, 27 th EPS, Budapest, 2000, paper P3.120.
[6] C. B. Forest et al., Physics of plasmas, Vol. 7, (2000), 1352.